Stereo-dynamics of the exchange reaction $H_a+LiH_b \rightarrow LiH_a+H_b$ and its isotopic variants*

Zhai Hong-Sheng(翟红生)[a] and Yin Shu-Hui(尹淑慧)[b]†

[a] *State Key Laboratory of Molecular Reaction Dynamics, Dalian Institute of Chemical Physics, Chinese Academy of Science, Dalian* 116023, *China*

[b] *Department of Physics, Dalian Maritime University, Dalian* 116026, *China*

(Received 20 March 2012; revised manuscript received 30 May 2012)

The quasi-classical trajectory (QCT) method is used to calculate the stereo-dynamics of the exchange reaction $H_a+LiH_b \rightarrow LiH_a+H_b$ and its isotopic variants based on an accurate potential energy surface reported by Prudente *et al.* [Prudente F V, Marques J M C and Maniero A M 2009 *Chem. Phys. Lett.* **474** 18]. The reactive probability of the title reaction is computed. The vector correlations and four polarization-dependent generalized differential cross sections (PDDCSs) at different collision energies are presented. The influences of the collision energy and the reagent rotation on the product polarization are studied in the present work. The results indicate that the product rotational angular momentum $\boldsymbol{j}'$ is not only aligned, but also oriented along the direction perpendicular to the scattering plane. The product polarization distributions of the title reaction and its isotopic variants exhibit distinct differences which may arise from different mass combinations.

Keywords: quasi-classical trajectory, reaction stereo-dynamics, vector correlation, reactive probability

PACS: 82.20.Bc, 82.20.Kh **DOI:** 10.1088/1674-1056/21/12/128201

1. Introduction

The extensive studies on the neutral and ionic LiH are done because of their potential importance in the primordial universe chemistry.[1−4] The comprehensive chemistry of lithium in the post-recombination epoch was presented by Stancil *et al.*,[5] and the abundances of Li, Li^+, Li^-, LiH, and LiH^+ were employed for calculation as a function of red-shift z for several cosmological models. Theoretical studies[6−9] on the spectroscopic, polarizability, and mono-bichromatic electron dynamics of LiH have been reported. Experimental investigations about the formation reaction of LiH of various electronic states have also been reported.[10,11] Bililign *et al.*[10] conducted laser induced pump-probe far-wing scattering experiments to study the photochemical reaction $Li+H_2 \rightarrow LiH+H$. Chen *et al.*[11] observed the nascent rotational population distribution of LiH in the atom Li and diatom molecule H_2 reaction by using a pump-probe technique.

During the past decade, the LiH_2 chemical system has attracted great attention to its potential energy surfaces (PESs),[12−20] and in the sub-reactive and reaction dynamic[3,12−15,21−26] of the highly exothermic reaction $LiH+H \rightarrow Li+H_2$ and the exchange reaction $H_a+LiH_b \rightarrow LiH_a+H_b$. The ground state potential energy surface (PES) of the LiH_2 system for the collinear arrangement was initially constructed by Clarke *et al.*[17] with the extensive valence bond (VB) non-orthogonal configuration interaction (CI) method. Dunne, Murrell and Jemmer (DMJ)[16] presented the first three-dimensional (3D) LiH_2 PES by fitting the CI *ab initio* points to an analytical function within the many-body expansion (MBE) formalism. Wernli *et al.*[13] reported on a new three-dimensional PES for the electronic ground state of reaction $LiH+H \leftrightarrow Li+H_2$. Their results confirmed the absence of a barrier along the path to the LiH depletion reaction. Bovino *et al.*[20] presented a quantum mechanical study on the exothermic reaction LiH+H based on a 3D PES reported by Wernli *et al.*[13] Prudente *et al.*[12] constructed an accurate potential energy surface for the ground electronic state of the LiH_2 system in which the DMJ PES[16] was improved by FCI/aug-cc-pVQZ *ab initio* calculation. The new

*Project supported by the National Natural Science Foundation of China (Grant No. 11105022) and the Fundamental Research Funds for the Central Universities (Grant Nos. 2011QN142 and 2012QN066).

†Corresponding author. E-mail: yinsh@dlmu.edu.cn

© 2012 Chinese Physical Society and IOP Publishing Ltd

PES gets rid of the unphysical well and leads to very different wave packet dynamics for both exothermic LiH+H→Li+H_2 and H_a+LiH_b→LiH_a+H_b reactions compared with the previous ones[21,22,27] on the DMJ PES. For the reaction channel H_a+LiH_b→LiH_a+H_b, the PES has a very low barrier (2.0 kcal/mol above the H+LiH asymptote) and a shallow well (0.3 kcal/mol below the H+LiH asymptote) in the collinear configuration. As the ∠HLiH (the angle between the bonds LiH_a and LiH_b) decreases, the low barrier gradually disappears and the well depth increases.

As mentioned above, a lot of studies have dealt with the scalar properties such as reactive probability, integral cross section, and rate constant. The vector properties of chemical reactions, such as velocities and angular momenta, can provide valuable information about chemical reaction stereo-dynamics.[28−43] It is helpful to better understand the fullest picture of the scattering dynamics by studying the vector properties.

To our knowledge, the vector properties of the exchange reaction H_a+LiH_b→LiH_a+H_b have not yet reported. In this paper, we carry out the quasi-classical trajectory (QCT) calculations based on the potential energy surface constructed by Prudente *et al.*[12] to study the stereo-dynamics of the title reaction and its isotopic variants:

H_a+LiH_b→LiH_a+H_b, (R1)
H+LiD→LiH+D, (R2)
D+LiH→LiD+H, (R3)
D_a+LiD_b →LiD_a+D_b. (R4)

The rest of this paper is organized as follows. In Section 2, a brief description of the theoretical method and computational detail are presented. Then the results and the discussion are given in Section 3. Finally, conclusions are drawn from the present study in Section 4.

2. Method

The QCT method used here is the same as that described in Refs. [27]–[44], which can solve the classical Hamilton equations for the nuclei motion in three dimensions. The Hamilton equations are numerically integrated in three dimensions with six order symplectic integration. To guarantee the conservations of the total energy and total angular momentum within an acceptable tolerance, the integration step size is fixed at 0.1 fs. The maximum impact parameter $b_{\max}$ for different collision energies are listed in Table 1. Batches of 10^5 trajectories are sampled for impact parameters ranging from 0 to $b_{\max}$.

The center-of-mass (CM) frame is chosen in this calculation as shown in Fig. 1. The z axis is parallel to initial relative velocity vector $\boldsymbol{k}$ whereas the y axis is perpendicular to the x–z plane containing the initial and final relative velocity vectors, $\boldsymbol{k}$ and $\boldsymbol{k}'$. θ is the angle between $\boldsymbol{k}$ and $\boldsymbol{k}'$ (so-called scattering angle). θ_r and φ_r are the polar and azimuthal angles of the final rotational angular momentum $\boldsymbol{j}'$.[39,40]

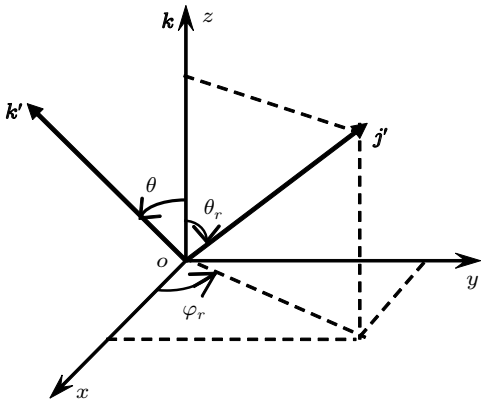


Fig. 1. Centre-of-mass frame describing the $\boldsymbol{k}$, $\boldsymbol{k}'$, and $\boldsymbol{j}'$ correlation.

The function $P(\theta_r)$ used to describe the $\boldsymbol{k}$–$\boldsymbol{j}'$ correlation can be expanded into a series of Legendre polynomials as[27,28]

$$P(\theta_r) = \frac{1}{2}\sum_m (2m+1)a_0^{(m)}\mathrm{P}_m(\cos\theta_r), \qquad (1)$$

where

$$\begin{aligned} a_0^m &= \int_0^\pi \mathrm{P}(\theta_m)\mathrm{P}_m(\cos\theta_r)\sin\theta_r\,\mathrm{d}\theta_r \\ &= \langle \mathrm{P}_m(\cos\theta_r)\rangle, \end{aligned} \qquad (2)$$

with the expanding coefficients a_0^m being called orientation (m is odd) or alignment (m is even) parameter and the angular brackets representing an average over all the reactive trajectories, $m = 2$ indicating the product rotational alignment expressed as

$$a_0^2 = \langle \mathrm{P}_2(\cos\theta_r)\rangle = \langle \mathrm{P}_2(\boldsymbol{j}'\cdot\boldsymbol{k})\rangle = \frac{1}{2}(3\cos^2\theta_r - 1). \qquad (3)$$

Here we calculate only the average rotational alignment of the product, as it has been measured in most experiments to date. In this article, $P(\theta_r)$ is expanded up to $k = 18$, which shows good convergence.

The dihedral angle distribution function $P(\varphi_r)$ describing $\boldsymbol{k}$–$\boldsymbol{k}'$–$\boldsymbol{j}'$ vector correlation can be expanded into a Fourier series[28] as follows:

$$\begin{aligned} P(\varphi_r) = \frac{1}{2\pi}\Bigg[1 &+ \sum_{\text{even},n\geq 2} a_n\cos(n\varphi_r) \\ &+ \sum_{\text{odd},n\geq 1} b_n\sin(n\varphi_r)\Bigg], \end{aligned} \qquad (4)$$

where

$$a_n = 2\langle\cos(n\varphi_r)\rangle, \quad b_n = 2\langle\sin(n\varphi_r)\rangle. \tag{5}$$

A set of generalized polarization-dependent differential cross sections (PDDCSs) is used to describe the full three-dimensional angular distribution associated with $\boldsymbol{k}$–$\boldsymbol{k}'$–$\boldsymbol{j}'$ correlation in the CM frame. The fully correlated CM angular distribution can be presented as a joint density function which is written in the summation form as[44]

$$P(\omega_t, \omega_r) = \sum_{q=-k}^{k} \frac{[k]}{4\pi} \frac{1}{\sigma} \frac{\mathrm{d}\sigma_{kq}}{\mathrm{d}\omega_t} C_{kq}(\theta_r, \varphi_r)^*, \tag{6}$$

where $[k] \equiv 2k+1$, $-k \le q \le k$ and $(1/\sigma)(\mathrm{d}\sigma/\mathrm{d}\omega_t)$ are the generalized PDDCSs, $C_{kq}(\theta_r, \varphi_r)$ are modified spherical harmonics. The angles $\omega_t = \theta$ and $\omega_r = \theta_r, \varphi_r$ refer to the coordinates of the unit vectors $\boldsymbol{k}'$ and $\boldsymbol{j}'$ along the directions of the product relative velocity angular momentum vectors in the CM frame, respectively. Many photo-initiated bimolecular reaction experiments are sensitive to only those polarization moments with $k = 0$ and $k = 2$. In this work, $(1/\sigma)(\mathrm{d}\sigma_{00}/\mathrm{d}\omega_t)$, $(1/\sigma)(\mathrm{d}\sigma_{20}/\mathrm{d}\omega_t)$, $(1/\sigma)(\mathrm{d}\sigma_{22+}/\mathrm{d}\omega_t)$, and $(1/\sigma)(\mathrm{d}\sigma_{21-}/\mathrm{d}\omega_t)$ are calculated with the computational method developed in Refs. [28]–[31]. In the computations, PDDCSs are expanded up to 7, which is sufficient for good convergence.

3. Results and discussion

Figure 2 shows the total reaction probability for total angular momentum $J = 0$ in a collision energy range of 0 eV–1.0 eV. In order to attest the validity of the QCT calculation, we carry out time-dependent wave packet calculation on the same PES to obtain the corresponding $J = 0$ quantum reaction probability. As can be seen, the results from the two calculations are in good agreement with each other.

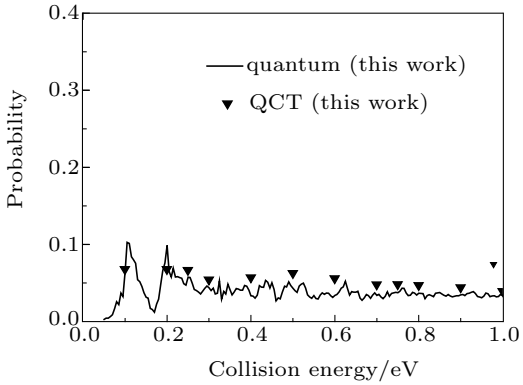


Fig. 2. Comparison of reactive probability between QCT and quantum calculations.

The distributions of $P(\theta_r)$ at three collision energies ($E_{\mathrm{col}} = 0.2$, 1.0, and 2.0 eV) for the four reactions R1–R4 are shown in Fig. 3. The $P(\theta_r)$ distributions, namely the rotational alignment of the product, describing the $\boldsymbol{k}$–$\boldsymbol{j}'$ correlation of the product LiH (LiD), peak at θ_r angles close to $\pi/2$ and are symmetric with respect to $\pi/2$, which demonstrates that $\boldsymbol{j}'$ is distributed with cylindrical symmetry in the product scattering frame and preferentially in the direction perpendicular to $\boldsymbol{k}$ direction. The $P(\theta_r)$ peak of reaction R3 which in Fig. 3(a) is the highest one, can prove that the rotational angular momentum vector of the product from reaction R3 mostly prefers to be perpendicular to the $\boldsymbol{k}$ vector. In Fig. 3, it can be

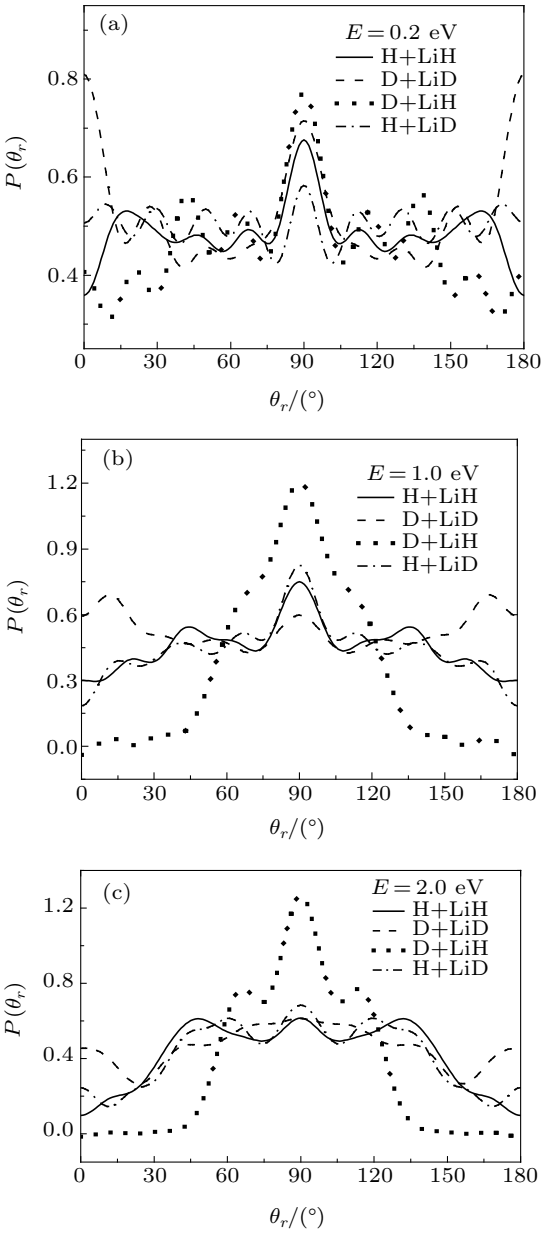


Fig. 3. $P(\theta_r)$ distributions for the reactions R1–R4 at the collision energies 0.2 (a), 1.0 (b), and 2.0 eV (c).

seen clearly that the peaks of $P(\theta_r)$ for reaction R3 are higher than those of reaction R1 at various collision energies. It illustrates that the angular momentum alignment of product molecule LiH is enhanced for the isotope D instead of the H atom. The peak of reaction R4 is higher than that of reaction R2 at the energy 0.2 eV and the peaks of the reaction R4 are lower than those of reaction R2 for the energies 1.0 eV and 2.0 eV. It indicates that the angular momentum alignment of product molecule LiD is enhanced for the H atom instead of the isotope D at low collision energy, while the alignment declines at the high collision energy. The peaks of $P(\theta_r)$ become higher as collision energy increases, which means that the degrees of the rotation and polarization of the product LiH (LiD) molecule are enhanced as collision energy increases. This is also confirmed by the values of the product rotational alignment parameter $\langle \mathrm{P}_2(\boldsymbol{j}' \cdot \boldsymbol{k}) \rangle$ for collision energies 0.2, 1.0, 2.0 eV in Table 2. This phenomenon is consistent with the calculations for LHL mass combination reaction on an attractive potential energy surface reported in Ref. [29] and Ref. [30].

Table 1. Maximum values of impact parameter $b_{\max}$ at different collision energies.

Collision	$b_{\max}$/Å			
energy/eV	H+LiH	H+LiD	D+LiH	D+LiD
0.1	4.41	4.70	4.13	4.28
0.2	4.10	4.09	3.78	4.05
0.3	3.80	3.73	3.64	6.65
0.4	3.50	3.62	3.40	3.48
0.5	3.50	3.30	3.37	3.23
0.6	3.49	3.32	3.50	3.23
0.7	3.49	3.33	3.49	3.34
0.8	3.49	3.30	3.51	3.35
0.9	3.49	3.31	3.51	3.34
1.0	3.49	3.30	3.51	3.35
1.1	3.49	3.30	3.52	3.32
1.2	3.49	3.30	3.51	3.29
1.3	3.49	3.23	3.51	3.28
1.4	3.51	3.23	3.51	3.27

Table 2. $P_2(\boldsymbol{j}' \cdot \boldsymbol{k})$ values of the reactions R1–R4 at different collision energies (0.2, 1.0, 2.0 eV).

Reaction	$P_2(\boldsymbol{j}' \cdot \boldsymbol{k})$		
	0.2 eV	1.0 eV	2.0 eV
H+LiH	−0.34427	−0.36850	−0.37808
H+LiD	−0.34685	−0.32137	−0.38408
D+LiH	−0.36918	−0.47999	−0.48192
D+LiD	−0.32997	−0.38014	−0.39349

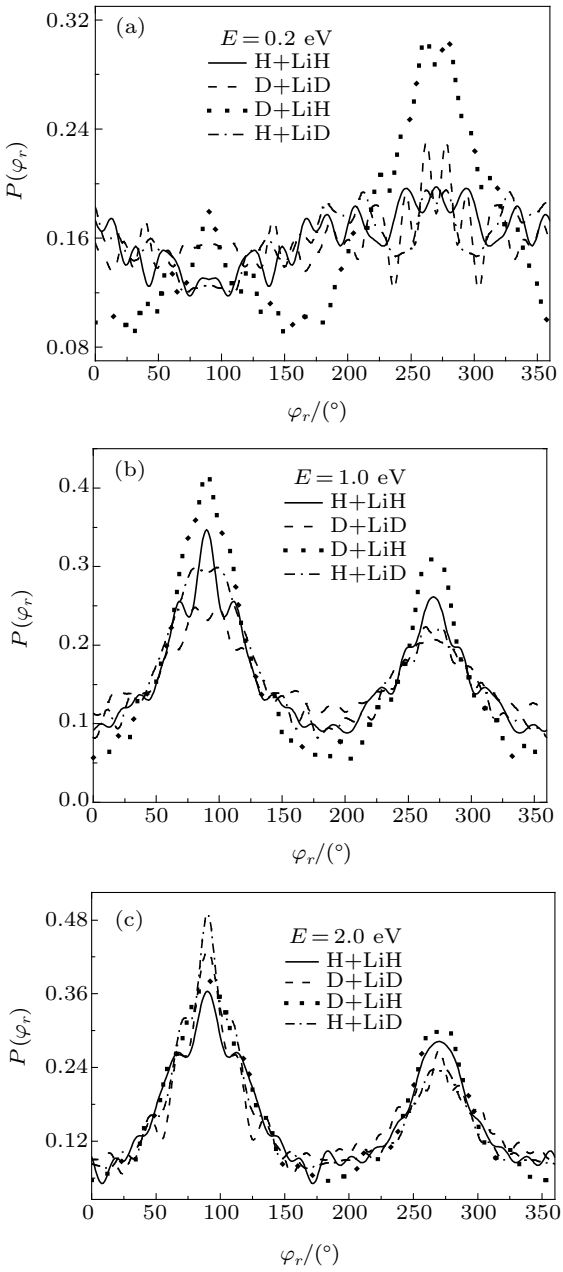


Fig. 4. $P(\varphi_r)$ distributions for the reactions R1–R4 at the collision energies 0.2 (a), 1.0 (b), and 2.0 eV (c).

Figure 4 shows the dihedral angle distributions $P(\varphi_r)$ of the four reactions for the collision energies at 0.2 eV, 1.0 eV, and 2.0 eV, which describe the $\boldsymbol{k}$–$\boldsymbol{k}'$–$\boldsymbol{j}'$ correlations. These distributions tend to be asymmetric with respect to the $\boldsymbol{k}$–$\boldsymbol{k}'$ scattering plane (about π), directly reflecting the strong polarization of product rotational angular momentum. The peaks of $P(\varphi_r)$ appear at $\pi/2$ and $3\pi/2$, showing that the rotational angular momentum vector of the product LiH (LiD) is oriented mainly along the y axis of the CM frame. Figure 4(a) shows the $P(\varphi_r)$ distributions for reactions R1–R4 at the low collision energy 0.2 eV. It can be distinctly seen that the $P(\varphi_r)$ peaks at $3\pi/2$ are

slightly larger than those at $\pi/2$, which reveals that the molecular products (LiH and LiD) are oriented preferentially along the negative direction of the y axis at the low collision energy. In Figs. 4(b) and 4(c), the peaks of the four reactions at $\pi/2$ are larger than those of $3\pi/2$ at the collision energies 1.0 eV and 2.0 eV. It indicates that the molecular product orientation along the y axis of the CM frame for the title reaction and isotopic variants gradually changes from the negative direction to positive direction and is enhanced in the positive direction with the increase of collision energy. As shown in Fig. 4, the peaks of the reaction R3 are higher than those of the reaction R1. It illustrates that the angular momentum orientation of product molecule LiH is enhanced for the isotope D instead of the H atom. The peak of the reaction R4 is higher than that of the reaction R2 at the energy 0.2 eV. In contrast, the peaks of the reaction R4 are lower than those of the reaction R2 at the energies 1.0 and 2.0 eV. This situation indicates that for the H atom instead of the isotope D, the angular momentum orientation of product molecule LiD is enhanced at low collision energy and declines at the high collision energy.

The generalized PDDCSs describe $\boldsymbol{k}$–$\boldsymbol{k}'$–$\boldsymbol{j}'$ correlation and the scattering direction of the product molecules. The PDDCS P_{00} distribution, which is proportional to the differential cross section (DCS), describes only the angular distribution of the product molecule. It is not related to the product orientation and alignment. The trajectory of P_{20} shows the opposite trend to that of P_{00}, which indicates the degree of alignment of the product rotational angular momentum $\boldsymbol{j}'$ being perpendicular to $\boldsymbol{k}$. The $\boldsymbol{k}$–$\boldsymbol{k}'$ scattering plane is $q \neq 0$ determined not by these limiting scattering angles, so the value of these PDDCSs with $q \neq 0$ should be zero at the extremities of backward and forward scatterings. The representation of PDDCSs with $q \neq 0$ for scattering away from the extreme forward and backward directions may be more attractive and can provide abundant dynamic information about the dihedral angle distribution.

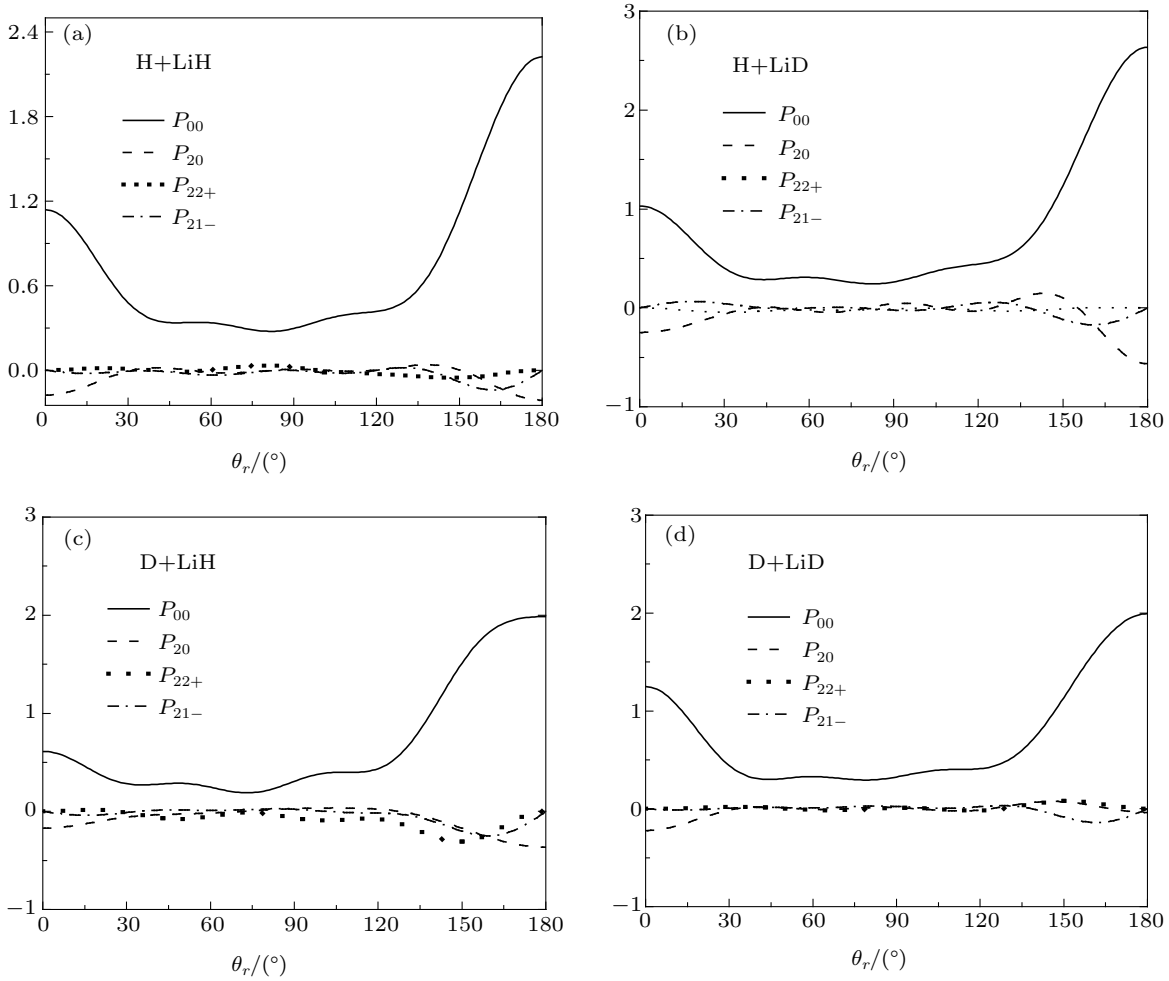


Fig. 5. Four PDDCSs with $P_{kq} = (P_{00},\ P_{20},\ P_{22+},\ P_{21-})$ for the reactions R1 (a), R2 (b), R3 (c), and R4 (d) at collision energy 0.2 eV.

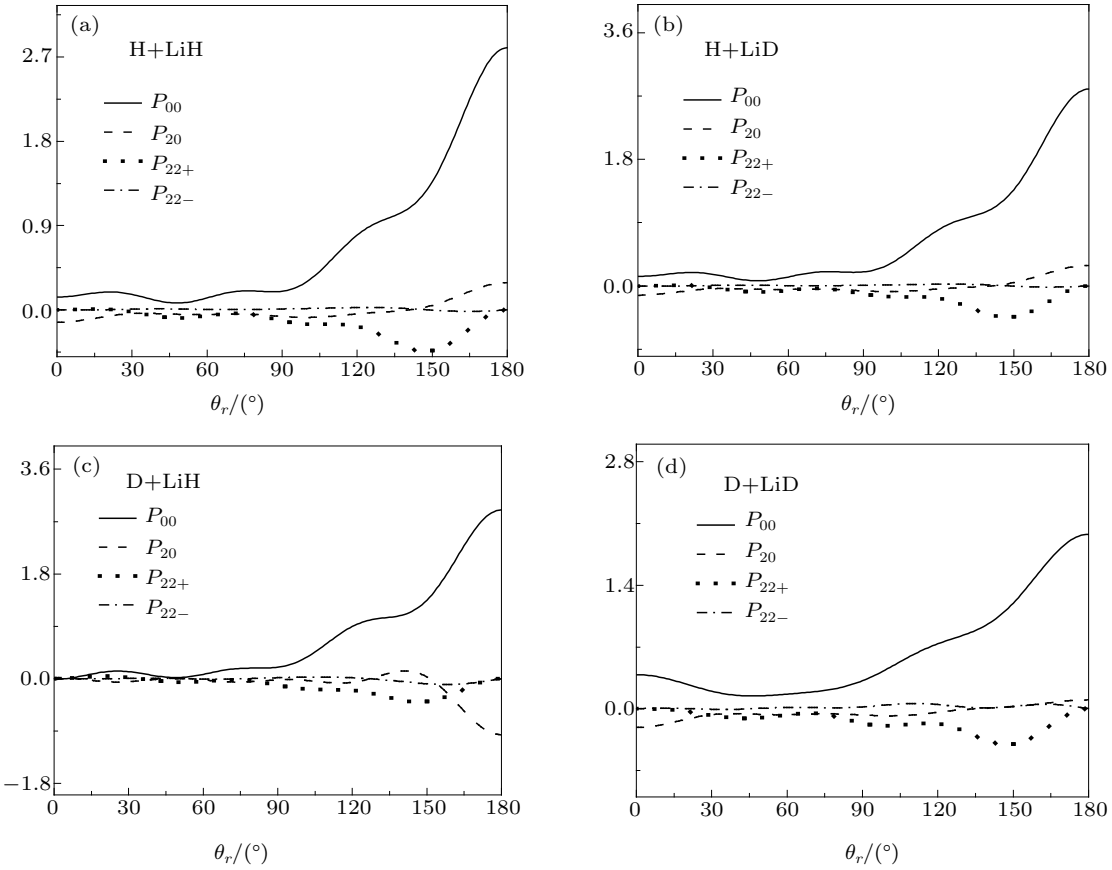


Fig. 6. The same as Fig. 5 except for the collision energy 1.0 eV.

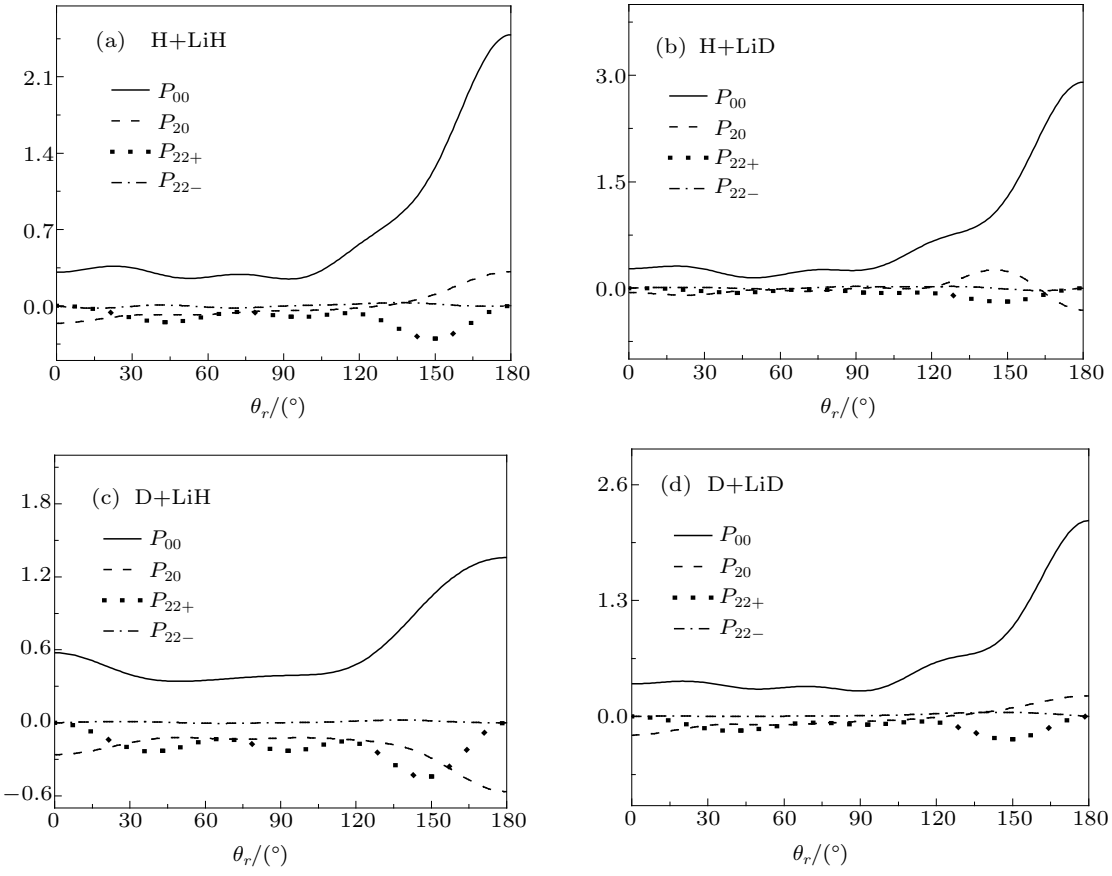


Fig. 7. The same as Fig. 5 except for the collision energy 2.0 eV.

Figures 5–7 show the PDDCSs for the four reactions at different collision energies 0.2, 1.0, and 2.0 eV. In Fig. 5, the four P_{00} distributions indicate that the product molecules are strongly scattered forward (in a scattering range of 0°–30°) and backward (in a scattering range of 135°–180°) for all four reactions. From the comparison of the P_{00} distribution between reactions R1 and R2, we can see that the sideways and forward scattering of product LiH in the reaction R1 are stronger than those of the reaction R2. While the sideways and forward scattering of product LiD in the reaction R3 are weaker than those in the reaction R4. The results demonstrate that the isotope effect depresses the product sideways and forward scattering. Figure 6 exhibits the PDDCSs for the four reactions at the collision energy 1.0 eV. The P_{00} distributions in the four reactions indicate that the product molecules are strongly scattered backward. The P_{20} distributions show that $\boldsymbol{j}'$ is weakly aligned in the direction perpendicular to $\boldsymbol{k}$ in a scattering angle range of 135°–180°. The PDDCSs with $q \neq 0$ of the four reactions are all close to zero. In Fig. 7, the product molecules of the four reactions are scattered backward in a scattering angle range of 135°–180°. The four P_{20} distributions indicate that each $\boldsymbol{j}'$ is weakly aligned in the direction perpendicular to $\boldsymbol{k}$ in the scattering angle range of 135°–180°, which is the same as the result in Fig. 6. It can be seen that the sideways and forward scatterings for the four reactions at the low collision energy are obviously stronger than those at high collision energy. It illustrates that the indirect reactive mechanism plays an important role at the low collision energy. This is due to the characteristic of PES that the title reaction goes through a well on the reactive path. As a whole, the direct reactions are predominant in the title reaction and its isotopic variants. The backward scattering enhances and dominates the reaction at the high collision energy. This is opposite to the exothermic reaction LiH+H→Li+H_2[23] which proceeds via a barrierless path on the PES.

4. Conclusions

The stereo-dynamics calculations of the exchange reactions H_a+LiH_b→LiH_a+H_b, H+LiD→LiH+D, D+LiH→LiD+H, and D_a+LiD_b →LiD_a+D_b are performed by using the QCT method. The reactive probabilities of the title reaction are computed. The results of QCT and quantum calculations are in good agreement with each other. The $P(\theta_r)$ distributions, $P(\varphi_r)$ distributions, and generalized PDDCSs of the four reactions for different collision energies are discussed in detail. The peaks of $P(\theta_r)$ become higher as collision energy increases. Owing to isotope effect, the angular momentum orientation of the product molecule is enhanced at the high collision energy. The angular momentum of the molecular product (LiH and LiD) aligns along the negative direction of the CM y axis for the title reaction and isotopic variants at the low collision energy. The alignment gradually changes from the negative direction to positive direction as collision energy increases. The results of the P_{00} distributions indicate the sideways and forward scatterings for the four reactions at the low collision energy are stronger than those at the high collision energy.

References

[1] Lepp S and Shull J M 1984 *Astrophys. J.* **280** 465

[2] Lepp S, Stancil P C and Dalgarno A 2002 *J. Phys.* B **35** 57

[3] Bodo E, Gianturco F A and Martinazzo R 2003 *Phys. Rep.* **384** 85

[4] Prodanovic T and Fields B D 2003 *Astrophys. J.* **597** 48

[5] Stancil P C, Lepp S and Dalgarno A 1996 *Astrophys. J.* **458** 401

[6] Yan Z C, Babb J F, Dalgarno A and Drake G W F 1996 *Phys. Rev.* A **54** 2824

[7] Hsu S K, Wang J J, Yu P, Wu C Y and Luh W T 2002 *J. Phys. Chem.* A **106** 6279

[8] Méawa M, Bégué D and Dargelos A 2003 *J. Phys. Chem.* A **107** 9628

[9] Acocella A, Jones G A and Zerbetto F 2006 *J. Phys. Chem.* A **110** 5164

[10] Bililign S, Hattaway B C, Robinson T L and Jeung G H 2001 *J. Chem. Phys.* **114** 7052

[11] Chen J J, Hung Y M, Liu D K, Fung H S and Lin K C 2001 *J. Chem. Phys.* **114** 9395

[12] Prudente F V, Marques J M C and Maniero A M 2009 *Chem. Phys. Lett.* **474** 18

[13] Wernli M, Caruso D, Bodo E and Gianturco F A 2009 *J. Phys. Chem.* A **113** 1121

[14] Martinazzo R, Tantardini G F, Bodo E and Gianturco F A 2003 *J. Chem. Phys.* **119** 11241

[15] Lee H S, Lee Y S and Jeung G H 1999 *J. Phys. Chem.* A **103** 11080

[16] Dunne L J, Murrell J N and Jemmer P 2001 *Chem. Phys. Lett.* **336** 1

[17] Clarke N J, Sironi M, Raimondi M, Kumar S, Gianturco F A, Buonomo E and Cooper D L 1998 *Chem. Phys.* **233** 9

[18] Kim K H, Lee Y S, Ishida T and Jeung G H 2003 *J. Chem. Phys.* **119** 4689

[19] Berriche H and Tlili C 2004 *J. Mol. Struct.* **678** 11

[20] Bovino S, Wernli M and Gianturco F A 2009 *Astrophys. J.* **699** 383

[21] Padmanaban R and Mahapatra S 2002 *J. Chem. Phys.* **117** 6469

[22] Padmanaban R and Mahapatra S 2004 *J. Chem. Phys.* **121** 7681

[23] Liu Y F, He X H, Shi D H and Sun J F 2011 *Comput. Theor. Chem.* **965** 107

[24] Defazio P, Petrongolo C, Gamallo P and Gonzáez M 2005 *J. Chem. Phys.* **122** 214303

[25] Shalabi A, Nour M and Halim W 2001 *J. Mol. Struct.* **541** 203

[26] Berriche H 2004 *J. Mol. Struct.* **682** 89

[27] Shafer-Ray N E, Orr-Ewing A J and Zare R N 1995 *J. Phys. Chem.* **99** 7591

[28] Han K L, He G Z and Lou N Q 1996 *J. Chem. Phys.* **105** 8699

[29] Wang M L, Han K L and He G Z 1998 *J. Chem. Phys.* **109** 5446

[30] Wang M L, Han K L and He G Z 1998 *J. Phys. Chem.* A **102** 10204

[31] Aoiz F J, Banares L and Herrero V J 1998 *J. Chem. Soc., Faraday Trans.* **94** 2483

[32] Bradley K S and Schatz G C 1997 *J. Chem. Phys.* **106** 8464

[33] Zhang L, Chen M D, Wang M L and Han K L 2000 *J. Chem. Phys.* **112** 3710

[34] Han K L, He G Z and Lou N Q 1993 *Chin. Chem. Lett.* **4** 517

[35] Ju L P, Han K L and Zhang J Z 2009 *J. Comput. Chem.* **30** 305

[36] Han K L, Zhang L, Xu D L, He G Z and Lou N Q 2001 *J. Phys. Chem.* A **105** 2956

[37] Lu Y C, Xiao J and Wang M S 2012 *Chin. Phys.* B **21** 043101

[38] Chen Y Y and Zhao M Y 2012 *J. Theor. Comput. Chem.* **11** 87

[39] Chen X Q, Wang M S, Yang C L and Wu J C 2012 *Chin. Phys.* B **21** 023402

[40] He X H, Liu Y F, Shi D H and Sun J F 2011 *Chin. Phys.* B **20** 078201

[41] Li H, Zheng B, Yin J Q and Meng Q T 2011 *Chin. Phys.* B **20** 123401

[42] Zhao J, Xu Y, Yue D G and Meng Q T 2009 *Chem. Phys. Lett.* **471** 160

[43] Xie T X, Li S J, Shi Y and Jin M X 2012 *Chin. Phys.* B **21** 013401

[44] Aoiz F J, Brouard M and Enriquez P A 1996 *J. Chem. Phys.* **105** 4964